Oxidative Transformation of Intermetallic Nanoparticles: An Alternative Pathway to Metal/Oxide Nanocomposites, Textured Ceramics, and Nanocrystalline Multimetal Oxides

Farah Dawood, Brian M. Leonard, and Raymond E. Schaak*

Department of Chemistry, Texas A&M University, P.O. Box 30012, College Station, Texas 77842-3012

Received April 27, 2007. Revised Manuscript Received June 8, 2007

A new low-temperature strategy is described for the synthesis of nanocrystalline multimetal oxides. In this approach, intermetallic nanoparticles synthesized via a modified polyol process are used as reactive precursors that help to define both the composition and morphology of multimetal oxides via a two-step thermal oxidation process. We use Bi_2PdO_4 and $Bi_2Pt_2O_7$ as model systems for elaborating this new synthetic strategy. For Bi_2PdO_4, intermetallic Bi_2Pd nanocubes are thermally oxidized to form a Bi_2O_3/Pd nanocomposite, which transforms to textured Bi_2PdO_4 upon further heating in O_2. $Bi_2Pt_2O_7$ is formed using a similar strategy involving the thermal oxidation of intermetallic Bi−Pt nanoparticles. The reaction pathway is established using a combination of X-ray diffraction analysis, transmission electron microscopy, thermogravimetric analysis, and energy-dispersive spectrometry element mapping data. Given the growing number of intermetallic compounds that are accessible as nanoparticles, this strategy has the potential to yield many other mixed metal oxides as nanocrystalline powders. Supported nanoparticle catalyst systems and textured ceramics are also accessible by exploiting the reaction pathway.

Introduction

The synthetic pathway that is used to make an inorganic solid-state material has a significant impact on many aspects of the final product. Issues of composition, crystal structure, phase purity, crystallinity, and homogeneity are a direct result of heating temperatures, heating profiles, and reagent stoichiometry, among other factors. Morphological characteristics such as crystallite size, shape, uniformity, and texture can also be influenced by temperature and heating profile, as well as by the use of additives, templates, and solution precursors. When combined, all of these factors—chemical, physical, and morphological—contribute to the usefulness of a material. Multimetal oxides are among the most frequently studied materials from the perspective of synthetic control.[1] For example, the synthetic variables mentioned above can be exploited to access complex multielement phases with narrow composition windows,[2] textured ceramics with properties that mimic those of single crystals,[3] crystals with properties that are critically dependent upon their purity and crystallinity,[4] and nanocrystalline solids with properties that differ from their bulk analogues.[5]

Here, we present an alternative strategy for synthesizing multimetal oxides, which exploits intermetallic nanoparticles as reactive precursors that help to define the composition and morphology of multimetal oxides via a two-step low-temperature oxidation process. This nanoparticle precursor strategy builds on three key synthetic capabilities. First, Bocarsly and co-workers reported that $PtCoO_2$ could be synthesized by thermal oxidation of a Pt−Co cyanogel precursor, which could also form PtCo alloys under inert atmospheres.[6] Similarly, Au−Zr alloys can be oxidized to form Au/ZrO_2 nanoparticle composites.[7] Second, our group has utilized nanoparticle composites as precursors for the low-temperature synthesis of alloys and intermetallic compounds,[8−10] as well as multimetal oxides.[11] In this approach, the nanoparticle composites effectively decrease diffusion distances to the nanometer scale, eliminating solid−solid diffusion as the rate-limiting step in the formation of solids and allowing solid-state reactions to occur faster and at lower temperatures than those required for traditional

* Corresponding author phone: (979) 458-2858; fax: (979) 845-4719; e-mail: schaak@mail.chem.tamu.edu.

(1) Rao, C. N. R.; Raveau, B. *Transition Metal Oxides*; VCH Publishers: New York, 1995.
(2) (a) Wang, J.; Monot, I.; Chaud, X.; Erraud, A.; Marinel, S.; Provost, J.; Desgardin, G. *Physica C* **1998**, *304*, 191−201. (b) Viapiana, M.; Schwitters, M.; Wouters, D. J.; Maes, H. E.; Van der Biest, O. *Mater. Sci. Eng., B* **2005**, *118*, 34−38.
(3) (a) Duran, C.; Trolier-McKinstry, S.; Messing, G. L. *J. Am. Ceram. Soc.* **2000**, *83*, 2203−2213. (b) Wang, Z.; Yushan, Y. *Chem. Mater.* **2001**, *13*, 1101−1107. (c) Li, S.; Li, Z.; Bozhilov, K. N.; Chen, Z.; Yan, Y. *J. Am. Chem. Soc.* **2004**, *126*, 10732−10737.
(4) (a) Mackenzie, A. P.; Haselwimmer, R. K. W.; Tyler, A. W.; Lonzarich, G. G.; Mori, Y.; Nishizaki, S.; Maeno. Y. *Appl. Phys. Lett.* **1998**, *80*, 161−164. (b) Zurbuchen, M. A.; Jia, Y.; Knapp, S.; Carim, A. H.; Schlom, D. G.; Zou, L. N.; Liu, Y. *Appl. Phys. Lett.* **2001**, *78*, 2351−2353.
(5) (a) Liu, Q.; Lu. W.; Ma, A.; Tang, J.; Lin, J.; Fang, J. *J. Am. Chem. Soc.* **2005**, *127*, 5276−5277. (b) Vestal, C. R.; Zhang, Z. J. *Chem. Mater.* **2002**, *14*, 3817−2822. (c) Malavasi, L.; Mozzati, M. C.; Polizzi, S.; Azzoni, C. B.; Flor, G. *Chem. Mater.* **2003**, *15*, 5036−5043.
(6) Heibel, M.; Kumar, G.; Wyse, C.; Bukovec, P.; Bocarsly, A. B. *Chem. Mater.* **1996**, *8*, 1504−1511.
(7) Sanz, N.; Lomello-Tafin, M.; Valmalette, J. C.; Isa, M.; Galez, Ph. *Mater. Sci. Eng., C* **2002**, *19*, 79−83.
(8) Sra, A. K.; Schaak, R. E. *J. Am. Chem. Soc.* **2004**, *126*, 6667−6672.
(9) Schaak, R. E.; Sra, A. K.; Leonard, B. M.; Cable, R. E.; Bauer, J. C.; Han. Y. -F.; Means, J.; Teizer, W.; Vasquez, Y.; Funck, E. S. *J. Am. Chem. Soc.* **2005**, *127*, 3506−3515.
(10) Leonard, B. M.; Schaak, R. E. *J. Am. Chem. Soc.* **2006**, *128*, 11475−11482.
(11) Henkes, A. E.; Bauer, J. C.; Sra, A. K.; Johnson, R. D.; Cable, R. E.; Schaak, R. E. *Chem. Mater.* **2006**, *18*, 567−571.

10.1021/cm071147t CCC: $37.00
Published on Web 08/02/2007

methods. Finally, we[8−10,12−16] and others[17,18] have been developing strategies for synthesizing a library of intermetallic nanoparticles with well-defined stoichiometries, particularly for intermetallics containing platinum group metals. Recent work also shows that it is possible to control the shape and size of intermetallic nanoparticles using solution chemistry strategies.[16]

When these synthetic capabilities are merged, an intriguing alternative strategy for synthesizing multimetal oxides becomes apparent. Binary intermetallic compounds of the late transition metals and post transition metals, which are becoming increasingly straightforward to synthesize as nanoparticles,[8−10,12−18] generally are line phases with well-defined stoichiometries. This implies that intermetallic nanoparticles could serve as single-source precursors for derivative compounds such as oxides, effectively defining the metal/metal ratios and providing uniform and homogeneous precursors with atomic-level mixing of the metal components in the correct ratios. Furthermore, under appropriate conditions, it is reasonable to anticipate that the shape and size of the intermetallic nanoparticles could be retained in the multimetal oxide product, serving as an interesting new strategy for controlling texture and morphology in complex oxide systems.

We demonstrate this synthetic pathway for two multimetal oxides: Bi_2PdO_4 and $Bi_2Pt_2O_7$. These initial targets were chosen because the intermetallic nanoparticle precursors with stoichiometries corresponding to those of known multimetal oxides are straightforward to synthesize and each system contains only one stable multimetal oxide. Bi_2PdO_4 is a semiconductor with tunable conductivity[19] and shows potential to be used in multilayer ceramic capacitor applications.[20] Pyrochlore-type $Bi_2Pt_2O_7$ is also a semiconductor and has been found to serve as a methanol oxidation catalyst for potential fuel cell applications.[21] Both Bi_2PdO_4 and $Bi_2Pt_2O_7$ are accessible as nanocrystalline solids by thermally oxidizing intermetallic Bi−Pd and Bi−Pt nanoparticles. When the intermetallic nanoparticles are heated in air or O_2, the bismuth oxidizes first, causing nanoscale phase separation into Bi_2O_3 and Pd/Pt. As nanocrystals, this occurs quite readily, facilitated by the high surface-to-volume ratio. When the intermetallic nanoparticles phase-separate into Bi_2O_3 and Pd/Pt, the two components remain within close proximity. In analogy to our earlier work involving the thermal transformation of similar phase-separated nanocomposites into homogeneous products via low-temperature diffusion,[8−11] one would predict that further heating will eventually facilitate oxidation of the Pd/Pt, followed by interdiffusion of the two binary oxides to form a homogeneous multimetal oxide. Indeed, the strategy appears to work well for the synthesis of Bi_2PdO_4 and $Bi_2Pt_2O_7$ and has the potential to be applicable to the synthesis of a large number of other multimetal oxides for which appropriate intermetallic nanoparticles are available as precursors. In addition, the nanocomposite intermediates consist of intimately mixed Pd/Pt and Bi_2O_3, which suggests that this reaction pathway could serve as an intriguing route to the preparation of oxide-supported metal nanoparticle catalysts. Also, the morphology of the multimetal oxide products appears to mimic the morphology of the intermetallic nanoparticle precursors, providing a strategy for deliberately introducing texture into multimetal oxide ceramics and also influencing the shapes and sizes of complex nanocrystalline oxides.

Experimental Section

Materials. The following chemicals were used as received: $Bi(NO_3)_3{\cdot}5H_2O$ from Mallinckrodt Chemical Works and K_2PtCl_6 (40.11% Pt), $PdCl_2$ (59.5% Pd), $NaBH_4$ (98%), poly(vinyl pyrrolidone) (PVP; MW = 40 000), and tetraethylene glycol (TEG; 99+%) from Alfa Aesar.

Synthesis. Nanoparticles of intermetallic Bi_2Pd and Bi−Pt were synthesized using a modified polyol process similar to one that has been previously reported.[13] For Bi_2Pd, 350 mg of PVP was dissolved in 15 mL of TEG using magnetic stirring under bubbling Ar for 1 h. The solution was then heated to 50 °C, and $PdCl_2$ (30.0 mg, 0.169 mmol dissolved in 15 mL of TEG) and $Bi(NO_3)_3{\cdot}5H_2O$ (164.1 mg, 0.3383 mmol dissolved in 5 mL of TEG) were simultaneously added to the solution followed by a freshly prepared solution of $NaBH_4$ (25.0 mg in 5 mL of TEG). Upon reduction, the solution turned black and was then heated to 280 °C for 3 h. The Bi−Pt (mixture of BiPt and Bi_2Pt) nanoparticles were synthesized by sequentially dissolving K_2PtCl_6 (24.0 mg, 0.0494 mmol), $Bi(NO_3)_3{\cdot}5H_2O$ (30.0 mg, 0.0618 mmol), and PVP (220 mg) in 25 mL of TEG using magnetic stirring and sonication. The solution was stirred vigorously under bubbling Ar for 1 h, after which a freshly prepared solution of $NaBH_4$ (25.0 mg in 5 mL of TEG) was slowly added to the solution while stirring. The solution turned black due to reduction and was heated to 215−220 °C. The products were collected by centrifugation and washed well with acetonitrile. Thermogravimetric analysis (TGA) analysis indicated that approximately 10% of the as-synthesized samples consisted of adsorbed solvent or polymer stabilizer. The as-made Bi_2Pd and Bi−Pt particles were first heated to 350 and 400 °C, respectively, in a tube furnace under O_2 to obtain the intermediate phase-separated products (Bi_2O_3/Pd and Bi_2O_3/Pt) and then to 780 and 700 °C, respectively, in O_2 to obtain the final Bi_2PdO_4 and $Bi_2Pt_2O_7$ products. Once the final temperatures were obtained, the products were held at that temperature for no longer than 5 min before being cooled down to room temperature. The lowest temperatures observed for accessing Bi_2PdO_4 and $Bi_2Pt_2O_7$ were 700 and 650 °C, respectively.

(12) Sra, A. K.; Ewers, T. D.; Schaak, R. E. *Chem. Mater.* **2005**, *17*, 758−766.
(13) Cable, R. E.; Schaak, R. E. *Chem. Mater.* **2005**, *17*, 6835−6841.
(14) Leonard, B. M.; Bhuvanesh, N. S. P.; Schaak, R. E. *J. Am. Chem. Soc.* **2005**, *127*, 7326−7327.
(15) Cable, R. E.; Schaak, R. E. *J. Am. Chem. Soc.* **2006**, *128*, 9588−9589.
(16) Chou, N. H.; Schaak, R. E. *J. Am. Chem. Soc.* **2007**, *129*, 7339−7345.
(17) (a) Roychowdhury, C.; Matsumoto, F.; Mutolo, P. F.; Abruna, H. D.; DiSalvo, F. J. *Chem. Mat.* **2005**, *17*, 5871−5876. (b) Roychowdhury, C.; Matsumoto, F.; Zeldovich, V. B.; Warren, S. C.; Mutolo, P. F.; Ballesteros, M. J.; Wiesner, U.; Abruna, H. D.; DiSalvo, F. J. *Chem. Mater.* **2006**, *18*, 3365−3372. (c) Alden, L. R.; Han, D. K.; Matsumoto, F.; Abruna, H. D.; DiSalvo, F. J. *Chem. Mater.* **2006**, *18*, 5591−5596. (d) Alden, L. R.; Roychowdhury, C.; Matsumoto, F.; Han, D. K.; Zeldovich, V. B.; Abruna, H. D.; DiSalvo, F. J. *Langmuir* **2006**, *22*, 10465−10471.
(18) Poudeu, P. F. P.; D'Angelo, J.; Kong, H.; Downey, A.; Short, J. L.; Pcionek, R.; Hogan, T. P.; Uher, C.; Kanatzidis, M. G. *J. Am. Chem. Soc.* **2006**, *128*, 14347−14355.
(19) (a) Bettahar, N.; Conflant, P.; Abraham, F. *J. Alloys Compd.* **1992**, *188*, 211−214. (b) Wang, S. F.; Hsu, Y. F. *Ceram. Int.* **2000**, *26*, 669−671.
(20) Wang, S. F.; Huebner, W. *J. Am. Ceram. Soc.* **1992**, *75*, 2339−2352.
(21) Beck, N. K.; Steiger, B.; Scherer, G. G.; Wokaun, A. *Fuel Cells* **2006**, *1*, 26−30.

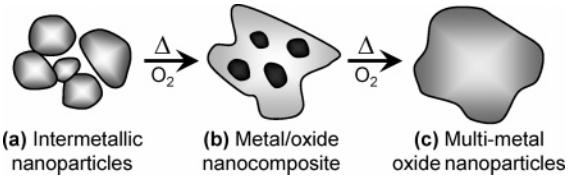

Figure 1. Schematic of the proposed reaction pathway for the formation of Bi_2PdO_4 and $Bi_2Pt_2O_7$ by the thermal oxidation of intermetallic Bi_2Pd and Bi−Pt nanoparticles. Partial oxidation of intermetallic nanoparticles initially yields a metal/oxide nanocomposite, which in turn transforms into the multimetal oxide nanoparticles.

Characterization. Powder X-ray diffraction (XRD) data were collected on a Bruker GADDS three-circle X-ray diffractometer (Cu Kα radiation). XRD data were also acquired using a Bruker AXS D8 Advance powder X-ray diffractometer (Cu Kα radiation). Transmission electron microscopy (TEM) images, selected area electron diffraction patterns, and an energy dispersive X-ray analysis (EDS) were collected using a JEOL JEM-2010 TEM. Elemental mapping images were acquired using a semi-STEM (STEM = scanning transmission electron microscopy) attachment. Samples were prepared by sonicating the isolated nanocrystalline powders in ethanol and dropping a small volume onto a carbon-coated nickel grid. TGA data were collected on a TA Instruments Q600 SDT under O_2 at a heating rate of 10 °C/min for Bi_2PdO_4 and 5 °C/min for $Bi_2Pt_2O_7$.

Results and Discussion

Oxidative Transformation of Intermetallic Nanoparticles. When metal nanoparticles are heated in an oxidizing environment, they convert to metal oxides, facilitated by the high surface area and also because many zerovalent metals (particularly 3d transition metals) are highly susceptible to oxidation.[22] Likewise, intermetallic nanoparticles can oxidize to multimetal oxides when heated in air or O_2. Because many intermetallic compounds are line phases that have a narrow composition range,[23] their utilization as stoichiometric precursors to multimetal oxides is particularly intriguing. Specifically, the composition of the multimetal nanoparticles can define the composition of the multimetal oxide, which is the product of the oxidative transformation. Figure 1 shows a schematic representation of the proposed reaction pathway that occurs upon the oxidative heating of intermetallic nanoparticles that contain a noble metal that is generally resistant to oxidation, such as Pd or Pt, and a heavy p-block element that is readily oxidized, such as Bi. First, intermetallic nanoparticles (e.g., Bi_2Pd or Bi−Pt) are formed by the $NaBH_4$ reduction of appropriate metal salts in TEG as described previously.[13] The intermetallic nanoparticles are then heated to 350−400 °C in O_2, which facilitates nanoscale phase separation of the nanoparticles, for example, into Bi_2O_3/Pd and Bi_2O_3/Pt. Further heating to 700−800 °C allows the noble metal to oxidize and react with the Bi_2O_3 to form nanocrystalline multimetal oxide products that have metal compositions matching those defined by the intermetallic nanoparticle precursors. It is anticipated that other intermetallic systems will also be amenable to oxidative transformation into multimetal oxides. For many of the intermetallic systems we have studied, few stable multimetal oxides are known. In these cases, phase separation into the binary oxides is common. For example, BiNi forms a mixture of nickel and bismuth oxides upon oxidation. Oxidation of BiPd produces Bi_2PdO_4 (the stable ternary oxide) plus extra bismuth oxide and Pd.

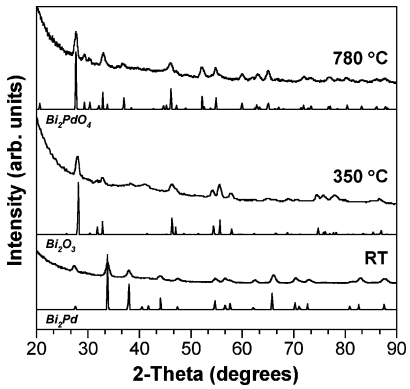

Figure 2. Powder XRD patterns showing the reaction pathway for the formation of Bi_2PdO_4. The intermetallic Bi_2Pd nanoparticles (RT) are heated to 350 °C in O_2, which convert to Bi_2O_3 and Pd. Further heating to 780 °C produces Bi_2PdO_4. Simulated patterns for β-Bi_2Pd, tetragonal Bi_2O_3, and Bi_2PdO_4 are shown below the appropriate experimental data.

Oxidative Transformation of Bi_2Pd into Bi_2PdO_4. The powder XRD data in Figure 2 show the Bi_2Pd precursor and the progression of crystalline phases that appear upon heating of the intermetallic Bi_2Pd nanoparticles in O_2. The XRD pattern for the Bi_2Pd nanoparticles matches well with that expected for β-Bi_2Pd (JCPDF no. 29-0232), showing no evidence of other crystalline phases. It is difficult to isolate a "perfect" intermediate as shown schematically in Figure 1b because the oxidation occurs continuously over a range of temperatures. Figure 2 shows XRD data for the intermediate isolated after heating Bi_2Pd nanoparticles to 350 °C in O_2 for 30 min. The predominant phase is tetragonal Bi_2O_3. Pd is not immediately evident in the XRD data, but the broad raised background centered near 41° 2θ is consistent with nanocrystalline or amorphous Pd. (TEM and EDS analysis, discussed later, confirms the presence of nanocrystalline Pd in the nanocomposite.) Further heating to 780 °C in O_2 for 40 min produces phase-pure Bi_2PdO_4. The lattice constants for Bi_2PdO_4 [a = 8.622(8) Å, c = 5.901(1) Å] agree favorably with prior reports (a = 8.614−8.623 Å, c = 5.816−5.909 Å).[24]

Semi-STEM element mapping (Figure 3) provides a direct look at the nanostructure and the distribution of elements throughout the reaction. Figure 3a shows a TEM micrograph of the intermetallic Bi_2Pd nanoparticles that are used as precursors. The nanoparticles are generally cube-shaped with diameters ranging from 40 to 60 nm. In analogy to other strategies for synthesizing metal nanocubes,[25] the presence of PVP and other metal cations in solution may have some

(22) Yin, M.; Wu, C. K.; Lou, Y.; Burda, C.; Koberstein, J. T.; Zhu, Y.; O'Brien, S. *J. Am. Chem. Soc.* **2005**, *127*, 9506−9511.

(23) Massalski, T. B., Ed. *Binary Alloy Phase Diagrams*; ASM International: Materials Park, OH, 1996.

(24) (a) Lazarev, V. B.; Shaplygin, I. S. *Zh. Neorg. Khim.* **1974**, *19*, 2388−2390. (b) Arpe, R.; Mueller-Buschbaum, H. *Z. Naturforsch., B: Chem. Sci.* **1976**, *12*, 1708−1709. (c) Boivin, J. C.; Conflant, P.; Thomas, D. *C. R. Acad. Sci., Paris C* **1976**, *282*, 749−751. (d) Conflant, P.; Boivin, J. C.; Thomas, D. *Rev. Chim. Miner.* **1977**, *14*, 249−255. (e) Kakhan, B. G.; Lazarev, V. B.; Shaplygin, I. S. *Zh. Neorg. Khim.* **1979**, *24*, 1663−1668.

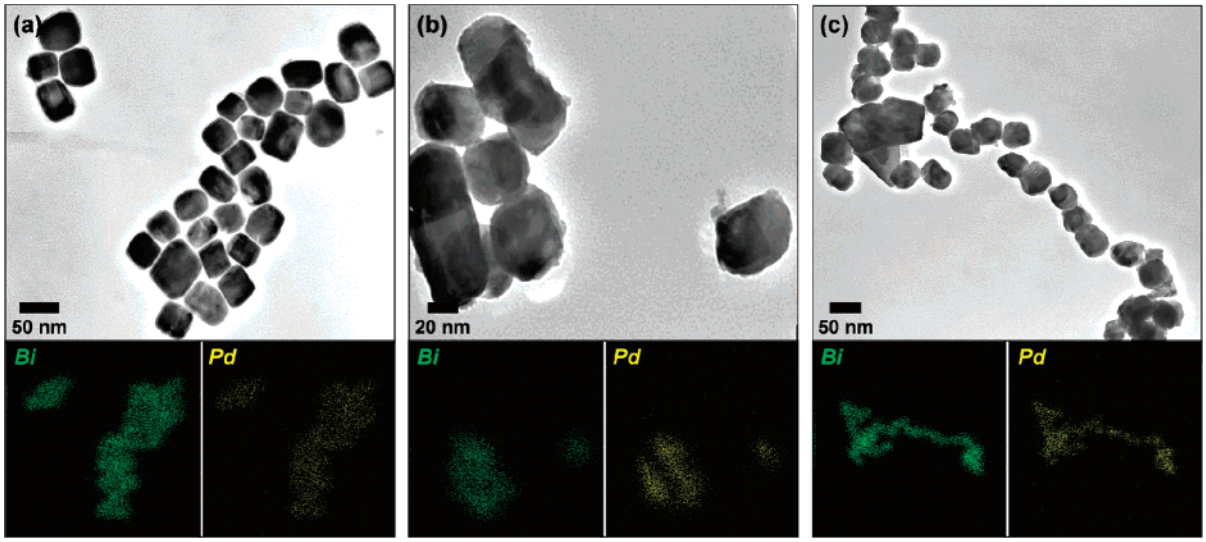

Figure 3. TEM micrographs and semi-STEM elemental mapping of (a) intermetallic Bi_2Pd nanoparticles, (b) the Bi_2O_3/Pd nanocomposite, and (c) the Bi_2PdO_4 product.

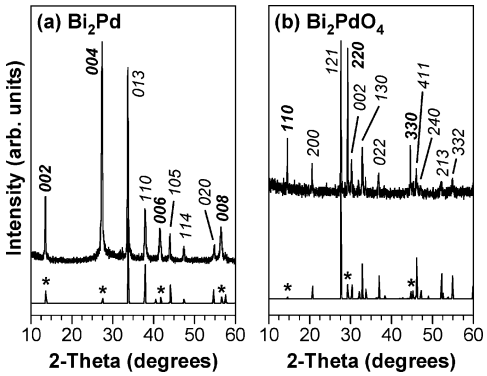

Figure 4. XRD patterns for oriented powders of (a) Bi_2Pd and (b) Bi_2PdO_4. Simulated XRD patterns are shown below the experimental data. The reflections indexed in boldface type and highlighted with an asterisk (*) indicate strong reflections due to preferred orientation along the <001> and <110> directions for Bi_2Pd and Bi_2PdO_4, respectively.

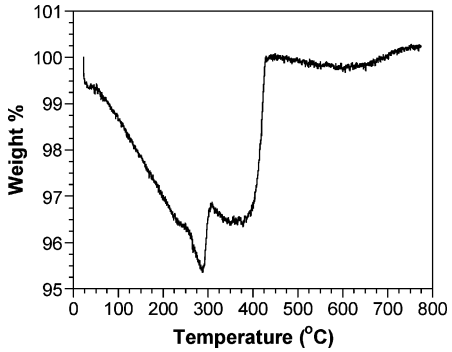

Figure 5. TGA data showing the weight change as intermetallic Bi_2Pd nanoparticles are thermally oxidized (in O_2) to form Bi_2PdO_4. The weight loss between room temperature and 300 °C is attributed to loss of surface-bound solvent, as well as oxidation and removal of the polymer stabilizer. The upturn in the TGA profile from 300 to 325 °C is due to the onset of Bi oxidation. As heating continues, the overall weight decreases due to competition between the weight gain (Bi oxidation) and weight loss (removal of polymer stabilizer), before increasing due to the final oxidation of Bi and Pd to form Bi_2PdO_4.

influence on the shape. On the basis of our prior work,[16] we hypothesize that Pd nanocubes form first and help to template cube-shaped Bi_2Pd. EDS confirms the 2:1 Bi/Pd stoichiometry, and element mapping (Figure 3a) confirms that the Bi and Pd are homogeneously distributed within the particles. After heating to 350 °C in O_2, the size and cube-shaped morphology of the particles do not change considerably (Figure 3b). However, element mapping (Figure 3b) shows clear segregation of the Bi and Pd components, with Pd localized in the centers of the cubes and Bi spread over the entire area (e.g., with Bi surrounding the Pd). EDS still shows a ~2:1 Bi/Pd ratio. This, combined with the XRD data, confirms the schematic shown in Figure 1b, specifically the occurrence of nanoscale phase separation to form a Bi_2O_3/Pd nanocomposite. After heating to 780 °C in O_2, the resulting Bi_2PdO_4 particles appear by TEM to retain their general size and cubic morphology (Figure 3c). Some particle agglomeration occurs (primarily via fusing of the nanoparticle surfaces), but it is likely minimized by the short (5−10 min) dwell times at the final reaction temperature. Element mapping (Figure 3c) confirms that the Bi and Pd are once again homogeneously mixed in the Bi_2PdO_4 product, providing visual evidence of the diffusion that occurred within the Bi_2O_3/Pd nanocomposite upon further heating.

Importantly, the progression of TEM micrographs for Bi_2Pd, Bi_2O_3/Pd, and Bi_2PdO_4 (Figure 3) shows a remarkable retention of morphology throughout the oxidative transformation. Powder XRD data show evidence of preferred orientation, which is also consistent with the morphology-conserving transformation observed by TEM. Figure 4a shows powder XRD data for a sample of Bi_2Pd nanocubes that was dispersed in ethanol and allowed to settle on a planar substrate. When compared to the simulated powder XRD pattern for β-Bi_2Pd, the experimental data show much higher intensities for the *002*, *004*, *006*, and *008* reflections (Figure 4a). This indicates that the nanocubes are preferentially oriented along the <001> direction. Powder XRD data for the Bi_2PdO_4 product show similar preferred orientation effects (Figure 4b). In this case, however, it is the *110*, *220*,

(25) (a) Kim, F.; Connor, S.; Song, H.; Kuykendall, T.; Yang, P. *Angew. Chem., Int. Ed.* **2004**, *43*, 3673−3677. (b) Song, H.; Kim, F.; Connor, S.; Somorjai, G. A.; Yang, P. *J. Phys. Chem. B.* **2005**, *109*, 188−193. (c) Xiong, Y.; Chen, J.; Wiley, B.; Xia, Y.; Yin, Y.; Li, Z. Y. *Nano Lett.* **2005**, *5*, 1237−1242.

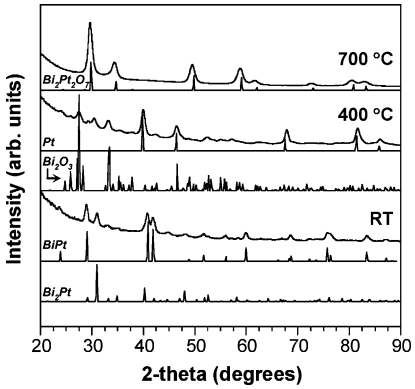

Figure 6. Powder XRD patterns characterizing the reaction pathway for the formation of $Bi_2Pt_2O_7$ by the thermal oxidation of intermetallic Bi−Pt nanoparticles using the optimal Bi/Pt ratio of 1.25:1.00. The intermetallic Bi−Pt nanoparticles are a mixture of BiPt and Bi_2Pt, as expected from the off-stoichiometry of the sample. Heating to 400 °C in O_2 shows the presence of Bi_2O_3 and Pt, and heating to 700 °C shows pyrochlore-type $Bi_2Pt_2O_7$. Simulated patterns for pyrochlore-type $Bi_2Pt_2O_7$, monoclinic Bi_2O_3, Pt, BiPt, and Bi_2Pt are shown below the appropriate experimental data.

and *330* reflections that are enhanced relative to the simulated pattern for Bi_2PdO_4. This indicates that the Bi_2PdO_4 product formed by thermal oxidation of the Bi_2Pd nanocubes also has an anisotropic texture, with preferential orientation along the <110> direction. Perfect cubes of Bi_2PdO_4 are certainly not generated by this approach, but the overall particle size and morphology are clearly related to the cube-shaped morphology of the Bi_2Pd precursor. This suggests that, if the morphology of intermetallic nanoparticles can be controlled, which growing evidence suggests is possible,[16] the morphology of multimetal oxide nanoparticles derived from these intermetallics should also be controllable when they are used as precursors. This strategy could therefore provide an alternative route for deliberately inducing texture in multimetal oxide ceramics.

TGA analysis (Figure 5) characterizing the thermal oxidation of intermetallic Bi_2Pd nanoparticles provides additional support to the proposed reaction pathway. The weight loss between room temperature and 300 °C is attributed to removal of surface-bound water and polyalcohol solvent molecules from the Bi_2Pd nanoparticles, as well as decomposition and volatilization of the polymer stabilizer used to prepare the Bi_2Pd nanoparticle precursors. (No measurable amount of carbon residue is present in the final Bi_2PdO_4 product, because combustion in O_2 facilitates its complete removal.) The upturn in the TGA profile from 300 to 325 °C is attributed to the onset of Bi oxidation to form Bi_2O_3. This weight increase due to oxidation competes with the weight loss due to continued removal of the polymer stabilizer, resulting in a net decrease in weight from 310 to 340 °C. From 400 to 430 °C, there is a significant weight gain, which is attributed to the complete oxidation of Bi to Bi^{3+} as well as the oxidation of Pd to Pd^{2+} (and the concomitant addition of oxygen to the sample). The slight weight gain above 430 °C is likely due to final oxidation of all of the Pd, as well as balance instability due to heat flux.

Oxidative Transformation of Bi−Pt into $Bi_2Pt_2O_7$. To provide evidence that the reaction pathway for converting intermetallic nanoparticles into multimetal oxides is general, we also studied the Bi−Pt system with the goal of preparing pyrochlore-type $Bi_2Pt_2O_7$. A representative powder XRD pattern for $Bi_2Pt_2O_7$ synthesized by heating intermetallic Bi−Pt nanoparticles to 700 °C in O_2 is shown in Figure S1 (Supporting Information). The XRD pattern matches that expected for pyrochlore-type $Bi_2Pt_2O_7$, and the lattice constant [a = 10.40(2) Å] agrees favorably with those previously reported for $Bi_2Pt_2O_7$ synthesized using other approaches [a = 10.36−10.37 Å].[26] Interestingly, phase-pure $Bi_2Pt_2O_7$ (as determined by laboratory XRD) is only obtained for Bi/Pt ratios of 1.25:1.00 or 1.30:1.00 (Figure S2, Supporting Information). A stoichiometric Bi/Pt ratio always yields a Pt impurity, and higher Bi/Pt ratios result in unreacted Bi_2O_3. (Refer to the Supporting Information for a discussion of the composition of $Bi_2Pt_2O_7$.) Since Bi−Pt intermetallic compounds are line phases with narrow composition limits, a 1.25:1.00 Bi/Pt ratio should give a mixture of BiPt and Bi_2Pt, on the basis of the Bi−Pt phase diagram.[23] As expected, the intermetallic nanoparticle precursor made with the 1.25:1.00 Bi/Pt ratio that yields phase-pure $Bi_2Pt_2O_7$ is indeed a mixture of BiPt and Bi_2Pt (Figure 6), with BiPt as the predominant phase. When heated to 400 °C in O_2,

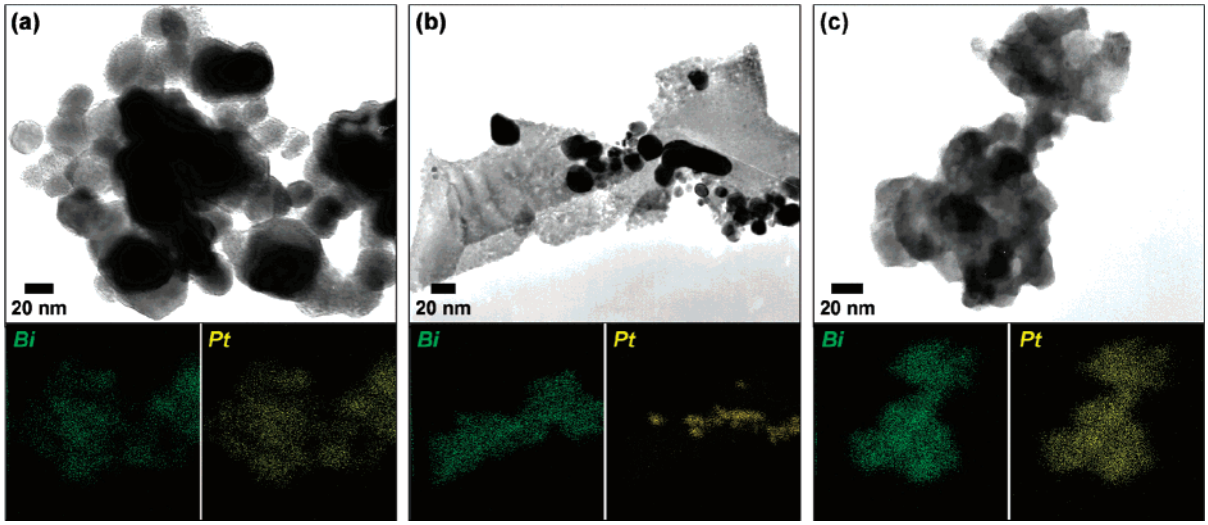

Figure 7. TEM micrograph and semi-STEM elemental mapping of (a) intermetallic Bi−Pt nanoparticles, (b) phase-separated Bi_2O_3/Pt, and (c) the nanocrystalline pyrochlore-type $Bi_2Pt_2O_7$ product.

the major phases are monoclinic Bi_2O_3 and face-centered cubic Pt, along with a small amount of unreacted Bi_2Pt (Figure 6). (Longer heating times at this temperature convert all of the Bi_2Pt to Bi_2O_3 and Pt.) Further heating to 700 °C produces phase-pure $Bi_2Pt_2O_7$, as determined by laboratory XRD.

The progression of crystalline phases upon the oxidation of intermetallic Bi−Pt nanoparticles mimics that of the Bi_2-Pd system. Likewise, TGA analysis characterizing the thermal oxidation of Bi−Pt nanoparticles (Figure S3, Supporting Information) shows the same features observed in the Bi_2Pd system: (a) initial weight loss due to the removal of surface-bound water and solvent, (b) weight loss due to polymer decomposition and volatilization, (c) weight gain due to the onset of Bi oxidation (competing with weight loss from polymer removal), and (d) weight gain due to the complete oxidation of Bi and Pt.

As for the Bi_2Pd system, element mapping shows nanoscale phase separation upon oxidation of the intermetallic Bi−Pt nanoparticles to form a Bi_2O_3/Pt nanocomposite, followed by transformation into $Bi_2Pt_2O_7$ nanoparticles (Figure 7). The TEM micrograph in Figure 7a shows the intermetallic BiPt/Bi_2Pt nanoparticles and the corresponding element map, which confirms that Bi and Pt are homogeneously distributed within the particles in a ∼1:1 Bi/Pt ratio. For the nanocomposite intermediate, phase separation in the Bi−Pt system is much easier to observe visually than in the Bi_2Pd system. In Figure 7b, the TEM micrograph shows dark particles that are largely spherical surrounded by a lighter-contrast phase with more well-defined edges (e.g., semicrystalline). Element mapping (Figure 7b) shows that the small dark particles are Pt and the surrounding material contains Bi, with almost no Pt. This provides direct evidence that Bi_2O_3 and Pt are phase-separated at the nanoscale. Interestingly, the morphology of the Pt nanoparticles surrounded by Bi_2O_3 is similar to that of many supported catalysts, where metal nanoparticles are dispersed among larger particles of a metal oxide. This reaction pathway that involves the oxidative transformation of intermetallic nanoparticles could provide a new route to supported metal nanoparticle catalysts, particularly for intermetallic systems that are rich in elements that are prone to oxidation. After heating to 700 °C, the Bi and Pt are once again homogeneously mixed in the $Bi_2Pt_2O_7$ product in a 1:1 ratio, which retains the nanocrystallinity, general size, and irregular morphology defined by the precursor (Figure 7c).

(26) (a) Sleight, A. W. *Mater. Res. Bull.* **1974**, *9*, 1177−1184. (b) Beck, E.; Kemmler-Sack, S. *J. Less-Common Met.* **1987**, *135*, 257−268. (c) Mayer-Von Kurthy, G.; Wischert, W.; Kiemel, R.; Kemmler-Sack, S.; Gross, R.; Huebener, R. P. *J. Solid State Chem.* **1989**, *79*, 34−45. (d) Takamori, T.; Boland, J. J. *J. Cryst. Growth* **1991**, *112*, 660−662.

Conclusions

Taken together, the presented data are consistent with a low-temperature multistep pathway that oxidatively transforms intermetallic nanoparticles into metal/oxide nanocomposites, which then transform into nanocrystalline multimetal oxides upon further heating. This result, demonstrated for the synthesis of Bi_2PdO_4 and $Bi_2Pt_2O_7$, shows that intermetallic nanoparticles (or mixtures of intermetallic nanoparticles) can serve as single-source precursors that define metal/metal stoichiometries that are maintained after oxidative transformation into a derivative phase. The high surface/volume ratio afforded by the intermetallic nanocrystals facilitates their reactivity, quickly phase-separating into nanoscale composites and readily diffusing without the need for higher temperatures. Given the growing number of intermetallic compounds that are accessible as nanocrystals,[8−10,12−18] this approach has the potential to be general for the synthesis of a wide range of mixed metal oxides, and possibly also for sulfides, nitrides, phosphides, and other types of solids using similar conversion strategies. Furthermore, the ability to generate metal/oxide nanocomposites as stable intermediates upon the thermal oxidation of intermetallic nanoparticles implies that this reaction pathway could serve as an alternative strategy for preparing supported catalysts, particularly for intermetallic nanoparticle precursors that are rich in easily oxidizing elements. Finally, the possibility of controlling the morphology of multimetal oxide systems by controlling the morphology of the intermetallic nanoparticle precursors (demonstrated for the Bi_2PdO_4 system) opens up a new route for designing shape-controlled oxide nanocrystals and textured ceramics.

Acknowledgment. This work was supported by a NSF CAREER Award (DMR-0545201), the Robert A. Welch Foundation (Grant No. A-1583), and start-up funds from Texas A&M University. Partial support was also provided by the Arnold and Mabel Beckman Foundation (Young Investigator Award), DuPont (Young Professor Grant), and the Texas Advanced Research Program (Grant No. 010366-0002-2006). Electron microscopy was performed at the Texas A&M Microscopy and Imaging Center.

Supporting Information Available: Additional characterization of $Bi_2Pt_2O_7$ (XRD, TGA, electron microprobe). This material is available free of charge via the Internet at http://pubs.acs.org.

CM071147T